2019 IEEE 16th International Symposium on Biomedical Imaging (ISBI 2019)
Venice, Italy, April 8-11, 2019

Human Knee Phantom for Spectral CT: Validation of a Material Decomposition Algorithm

S. Bussod ⋆, J.F.P.J. Abascal ⋆, N. Ducros ⋆, C. Olivier ⋆†, S. Si-Mohamed ⋆, P. Douek ⋆, C. Chappard ◇, F. Peyrin ⋆†

⋆ Univ. Lyon, INSA-Lyon, Université Claude Bernard Lyon 1, UJM Saint-Etienne, CREATIS CNRS UMR 5220, Inserm U1206, F-69621, Lyon, France

† The European Synchrotron Radiation Facility, Grenoble, France

◇ B2OA, UMR CNRS 7052, University Paris Diderot, Paris, France

ABSTRACT

Osteoarthritis is the most common degenerative joint disease. Spectral computed tomography generates energy-resolved data which enable identification of materials within the sample and offer improved soft tissue contrast compared to conventional X-ray CT. In this work, we propose a realistic numerical phantom of a knee to assess the feasibility of spectral CT for osteoarthritis. The phantom is created from experimental synchrotron CT mono-energetic images. After simulating spectral CT data, we perform material decomposition using Gauss-Newton method, for different noise levels. Then, we reconstruct virtual mono-energetic images. We compare decompositions and mono-energetic images with the phantom using mean-squared error. When performing material decomposition and tomographic reconstruction, we obtain less than 1 % error for both, using noisy data. Moreover, it is possible to see cartilage with naked eye on virtual mono-energetic images. This phantom has great potential to assess the feasibility and current limitations of spectral CT to characterize knee osteoarthritis.

***Index Terms*—** Spectral computed tomography, Material decomposition, Knee phantom, Osteoarthritis

1. INTRODUCTION

Osteoarthritis (OA) is the most common degenerative joint disease [1]. It is characterized by a cartilage loss, subchondral bone changes and joint narrowing [2]. It is most commonly diagnosed using imaging based on radiography but there are no current imaging techniques that provide direct visualization of both bone and cartilage [2]. Different modalities have been proposed to visualize cartilage integrity like sodium magnetic radiation imaging (MRI), computed tomography (CT) arthrography [1] and spectral CT (SCT) [3]. The potential of SCT has already been investigated for cardiovascular disease [4], among other applications [5]. Recently, it has been proposed for detecting OA using contrast agent [3]. Assessing the feasibility of SCT without contrast agent for OA has clinical relevance, and it has not been addressed.

Color X-ray or SCT is a new imaging modality exploiting energy-resolved data, thanks to photon counting (PC) detectors, providing higher contrast in soft tissue and higher resolution than conventional X-rays imaging. It even allows the reconstructed image to be decomposed into material constituents [6, 7].

The material decomposition problem is a nonlinear and ill-posed inverse problem. It is also non-convex because of the forward operator non-linearity [8]. A Gauss-Newton (GN) algorithm with material-specific regularization has been shown to be computationally efficient and to outperform the conventional maximum likelihood approach [9].

The main objective of this work is to present a numerical phantom of the human knee and to assess GN algorithm for the OA application.

The phantom is created by segmenting monochromatic synchrotron radiation (SR) CT data into different materials and assigning linear attenuation coefficients (LACs) for each material. Then, projections are simulated at different noise levels and decomposed using GN method [9], and volumes are reconstructed using filtered back-projection. Virtual mono energetic images (monoEs) are created for 40, 70 and 100 keV.

2. PHANTOM

2.1. Image acquisition

Knee samples are taken from the Institut d'Anatomie Paris Descartes and provided by B2OA (Bioingénierie et Bioimagerie ostéo-articulaire) CNRS 7052, Paris Diderot University. The study is approved by the ethics committee of Descartes University, Paris. Data on the same sample were

We thank ESRF staff members Herwig Requardt, Alberto Mittone, and Alberto Bravin for their support during the ESRF experiment MD-1045. We are also grateful to those that helped us during the experiment: Stephanie UK, Olga Kochebina, Claude Goubet, Florian Rousset, Gaelle Mitton, Odran Pivot, Tom Hohweiller, Adrien Halty, Hussein Banjak, Cyril Mory and Simon Rit. We acknowledge the support of the ANR project SALTO (ANR-17-CE19-0011-01). It was also performed within the framework of the LabEx PRIMES (ANR-11-LABX-0063) of Université de Lyon. The project has also received funding from the European Union's Horizon 2020 research and innovation program under the grant agreement N° 668142 and from the European Union's Horizon 2020 research and innovation program under the Marie Sklodowska-Curie grant agreement N° 701915.

acquired both with a Philips SCT prototype at CERMEP, Lyon [11] and with synchrotron CT at the European Synchrotron Radiation Facility (ESRF), Grenoble.

SR CT allows monoEs to be acquired experimentally [12]. Thus, these data are used as reference and for building the phantom. 3D SR CT images are acquired at high resolution (50 μm pixel size) and at energies 55, 75 and 100 keV. SCT data are acquired using a energy source with 120 kVp and 100 mA and a five bins detector. SCT images are used to validate simulated data. Reconstructed slices (zoomed) from SCT and SR CT are illustrated in Fig.2.

2.2. Phantom generation, data simulation and reconstruction of monoEs

Our realistic numerical phantom is built from the SR CT image at 55 keV. We automatically segment bone from soft tissue using thresholding. Cartilage is not segmented as it is visible with naked eye in the soft tissue image. Then, we use mass attenuation coefficients of soft tissue and bone from the NIST database [13] in order to compute the mass density for each material. Taking into account mass attenuation coefficients, we project mass densities and simulate PC data based on (4), using Spectral X-ray image reconstruction toolbox (SPRAY) [10]. Since synchrotron spatial resolution is high (50 μm), we downsample SR CT images to reach a final resolution of 240 μm. Projections are done using Radon transform from MATLAB, assuming parallel geometry with 720 projections along 180° (one projection each 0.25°) and two levels of noise are simulated using a Poisson distribution with $N_0 = 10^8$ and $N_0 = 10^6$.

Once projections in the different energy bins are calculated, material decomposition is performed using GN [9, 10]. MonoEs reconstruction is conducted as described in section 3.4.

3. SPECTRAL CT

3.1. Forward model

We assume a sensor with P pixels and I energy bins and an object with V voxels made of M materials that we image with Θ projections. Let $\mathbf{s} = (s^1_{1,1}, \ldots, s^\theta_{i,p}, \ldots, s^\Theta_{I,P})^\top$ be the measurement vector, where $s^\theta_{i,p}$ is the data measured in the i-th energy bin at the p-th pixel for the θ-th projection, and $\boldsymbol{\rho} = (\rho_{1,1}, \ldots, \rho_{m,v}, \ldots, \rho_{M,V})^\top$ be the (unknown) mass densities vector, where $\rho_{m,v}$ is the mass density for the m-th material at the v-th voxel. We note

$$\mathbf{s} = G(\boldsymbol{\rho}) \tag{1}$$

where G represents the forward model that maps $\boldsymbol{\rho}$ onto $\mathbf{s}$. The goal of SCT is to invert (1).

3.2. Projection-based interpretation

The forward model G can be seen as the composition of the X-ray transform X and a spectral mixing operator F.

The X-ray transform X applies to each material $\boldsymbol{\rho}_m$ independently, i.e.,

$$\mathbf{a}_m = X(\boldsymbol{\rho}_m), \quad 1 \leq m \leq M \tag{2}$$

with $\boldsymbol{\rho}_m = (\rho_{m,1}, \ldots, \rho_{m,v}, \ldots, \rho_{m,V})^\top$ and $\mathbf{a}_m$ represents the projected mass density for the m-th material $\mathbf{a}_m = (a^1_{m,1}, \ldots, a^\theta_{m,p}, \ldots, a^\Theta_{m,P})^\top$.

The spectral mixing F applies to each view independently, i.e.,

$$\mathbf{s}^\theta = F(\mathbf{a}^\theta), \quad 1 \leq \theta \leq \Theta \tag{3}$$

where $\mathbf{a}^\theta = (a^\theta_{1,1}, \ldots, a^\theta_{m,p}, \ldots, a^\theta_{M,P})^\top$. In particular, we consider the following non linear mixing [9]

$$s^\theta_{i,p} = \int_{\mathcal{E}} n_0(E) d_i(E) \, \exp\left[- \sum_{m=1}^{M} a^\theta_{m,p} \tau_m(E) \right] \mathrm{d}E \tag{4}$$

where $\mathcal{E}$ is the energy range of the source, n_o is the source energy spectrum, d_i is the detector response function of the i-th bin, and τ_m is the m-th material mass attenuation coefficient.

3.3. Inverse problems

3.3.1. *Material decomposition*

Material decomposition aims to invert (3). As in [9], we seek the solution by minimizing

$$C(\mathbf{a}^\theta) = \frac{1}{2} \, ||F(\mathbf{a}^\theta) - \mathbf{s}^\theta||^2_{\mathbf{W}} + \beta \left(\, ||\Delta \mathbf{a}^\theta_{\text{soft}}||^2_2 + ||\nabla \mathbf{a}^\theta_{\text{bone}}||^2_2 \, \right), \tag{5}$$

where the first term is the weighted least squares data fidelity term with $\mathbf{W} = \mathrm{diag}(1/\mathbf{s}^\theta)$ and the second term is the regularization term with β being the regularization parameter. Regularization consists in first- and second-order Tikhonov regularization for bone and soft-tissue, respectively, which promotes smooth solution and has a denoising effect.

To minimize (5), we used the GN method implemented in the MATLAB toolbox SPRAY [9, 10].

3.3.2. *Tomographic image reconstruction*

Having performed material decomposition and obtained $\mathbf{a}^\theta$, $1 \leq \theta \leq \Theta$, we reconstruct each material independently by inverting (2) with a filtered back-projection (FBP) algorithm using a Ramp filter.

3.4. MonoEs computation

Having performed the tomographic reconstruction and obtained $\boldsymbol{\rho}_m$, $1 \leq m \leq M$, we compute the monoEs as

$$\boldsymbol{\mu}(E) = \sum_{M} \boldsymbol{\rho}_m \tau_m(E) \tag{6}$$

where τ_m is the mass attenuation coefficient of the m-th material.

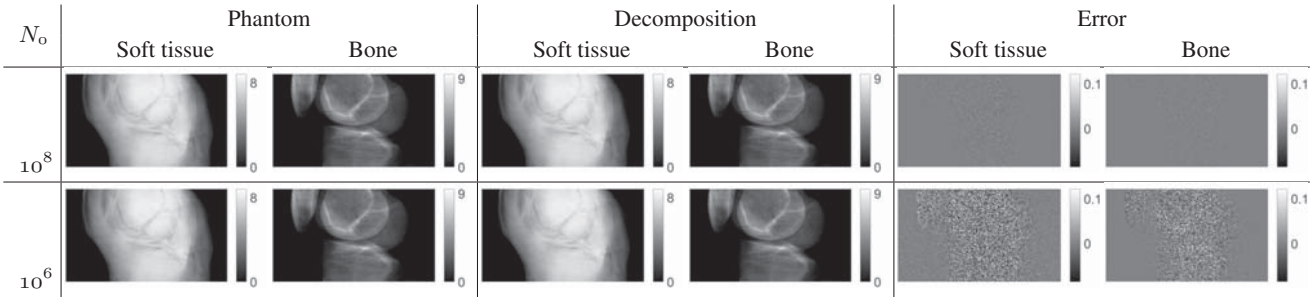

Fig. 1. Two materials decomposition, soft tissue and bone, for two different noise levels (projection 75°).

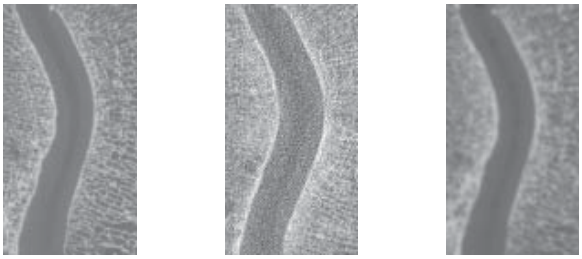

Fig. 2. Zoom in the cartilage area, μ values for experimental synchrotron 55 keV monoE (left), experimental SCT 70 keV monoE (center) and phantom 70 keV monoE (right).

		$N_0 = 10^8$	$N_0 = 10^6$
Material decomposition			
MSE	Soft tissue	$7.1\ 10^{-5}$	$4.0\ 10^{-3}$
	Bone	$\mathbf{3.0\ 10^{-5}}$	$1.7\ 10^{-3}$
Reconstructed monoEs			
MSE	40 keV	$1.2\ 10^{-4}$	$3.5\ 10^{-3}$
	70 keV	$\mathbf{9.6\ 10^{-8}}$	$6.9\ 10^{-4}$
	100 keV	$1.8\ 10^{-7}$	$\mathbf{4.3\ 10^{-4}}$

Table 1. Quantitative results for material decomposition and tomographic reconstruction.

4. RESULTS

4.1. Material decomposition

The result of two materials decomposition, simulating with two materials (bone and soft tissue), is shown in Fig.1.

Table 1 shows the mean square error (MSE) between decomposed projections and ground truth for two levels of noise. Increasing the level of noise from $N_0 = 10^8$ to $N_0 = 10^6$ leads only a two-fold increase in MSE. Decomposed images maintain similar image quality thanks to regularization.

4.2. MonoEs

In the Fig.2, we have a zoom in the patello femoral joint. Images show that cartilage can be seen with naked eye with SCT. The contrast between soft tissue and cartilage is as good for our phantom as for experimental images. However, our phantom is blurred, certainly caused by the effect of FBP while experimental SCT images are reconstructed using sharp filtering.

Reconstructed FBP monoEs are shown in Fig.3. At the lowest energy (40 keV), contrast is low. Images for 70 keV present the lowest error. Reconstructed images for $N_0 = 10^6$ photons are noisier and present streak artifacts, with worst performance for 40 keV.

In the Table 1, we can see that 70 keV yields lowest MSE for noiseless data and close to lowest error for the noisier data set. 100 keV and 70 keV provide high image quality overall.

5. DISCUSSION AND CONCLUSION

We proposed a human knee phantom to assess SCT algorithms for OA. We created the phantom for one knee sample and defined a workflow that can be applied to other knee samples. The workflow permits realistic simulation of PC data by modelling the scanner source spectrum, the detector response function and LACs of components of the knee. It also provides decomposed materials and reconstructed monoEs. The material decomposition of soft tissue and bone was successfully performed with RGN algorithm. Our results show that reconstructed monoE images at 70 keV and 100 keV provide the best image quality to assess cartilage integrity.

This is the first phantom created in order to validate SCT for osteoarthritic knee. To the best knowledge of the authors, this is the first time that SCT is shown to provide visualization of cartilage with sufficient resolution and image quality, which is not possible with conventional CT. In the future, we will use this phantom for characterizing the sensibility of the current SCT prototype for early detection of OA. In addition, this study could lead to define the requirements of SCT in terms of noise and sensitivity as well as to optimize scanner parameters such as energy thresholds, radiation dose in X-ray and reconstruction hyperparameters.

This study faces few limitations. Through visual inspection, we compared simulated monoEs from the phantom to those provided by the scanner. The contrast is similar for

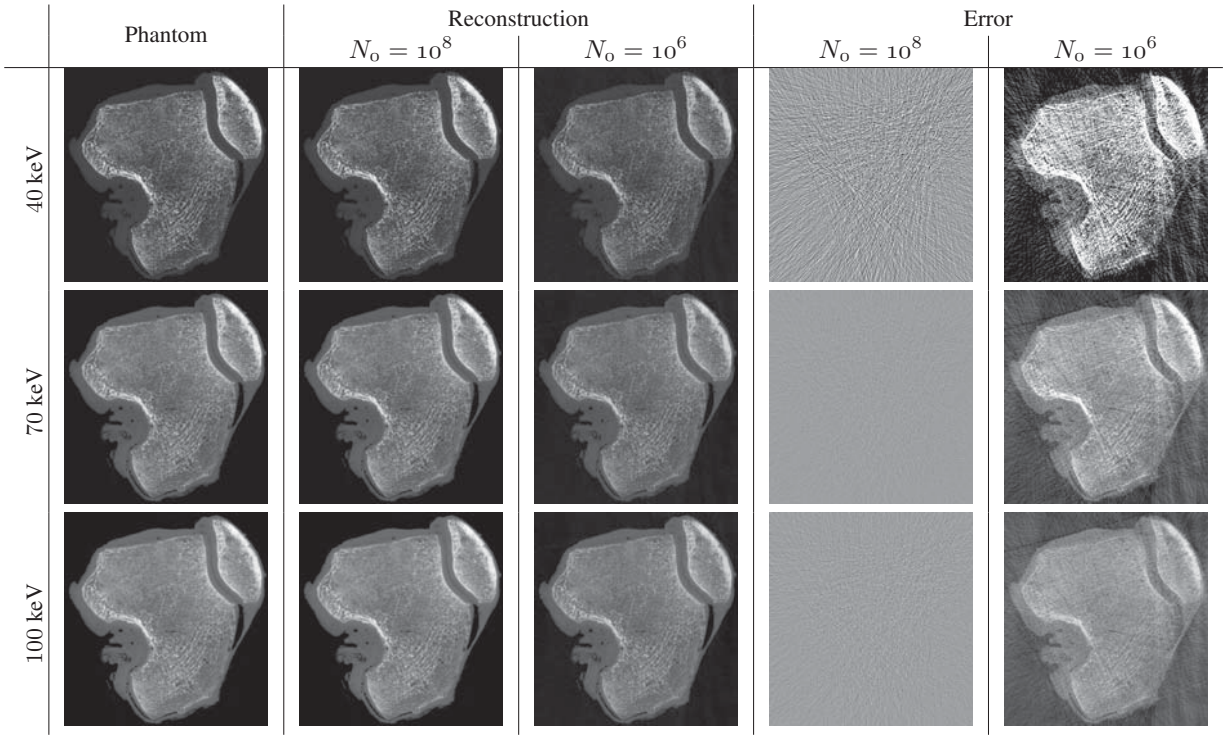

Fig. 3. MonoEs reconstruction for three energies and at two levels of noise.

simulation and experimental data. Further work will focus on quantitative validation of forward and inverse solutions against SCT experimental data. In addition, in this work we validated GN for two materials only. Further work will consider three materials, including cartilage.

In conclusion, we proposed a new realistic numerical phantom of the human knee and assessed two materials decomposition using GN algorithm. We also showed that reconstructed monoEs provide viable cartilage visualization. The proposed phantom, being the first of this kind, has great potential to assess the feasibility of spectral CT for OA.

6. REFERENCES

[1] E.H.G. Oei et al., "Quantitative Radiologic Imaging Techniques for Articular Cartilage Composition: Toward Early Diagnosis and Development of Disease-Modifying Therapeutics for Osteoarthritis," *Arthritis Care & Research*, vol. 66, no. 8, pp. 1129–1141, 2014.

[2] A. Guermazi et al., "Role of imaging in osteoarthritis: diagnosis, prognosis, and follow-up," Oct. 2013.

[3] K. Rajendran et al., "Quantitative imaging of excised osteoarthritic cartilage using spectral CT," *European Radiology*, vol. 27, May 2016.

[4] D.P. Cormode et al., "Atherosclerotic plaque composition: analysis with multicolor CT and targeted gold nanoparticles," *Radiology*, vol. 256, no. 3, pp. 774–782, Sept. 2010.

[5] B.J. Heismann et al., *Spectral Computed Tomography*, SPIE Press, 2012.

[6] K. Taguchi and J.S. Iwanczyk, "Vision 20/20: Single photon counting x-ray detectors in medical imaging," *Medical Physics*, vol. 40, no. 10, pp. 100901, Oct. 2013.

[7] J.P. Schlomka et al., "Experimental feasibility of multi-energy photon-counting K-edge imaging in pre-clinical computed tomography," *Physics in Medicine and Biology*, vol. 53, no. 15, pp. 4031–4047, Aug. 2008.

[8] J.F.P.J. Abascal et al., "Nonlinear material decomposition using a regularized iterative scheme based on the bregman distance," vol. 34, no. 12, pp. 124003, 2018.

[9] N. Ducros et al., "Regularization of Nonlinear Decomposition of Spectral X-ray Projection Images," *Medical Physics*, vol. 44, no. 9, pp. e174–e187, 2017.

[10] S. Si-Mohamed et al., "Review of an initial experience with an experimental spectral photon-counting computed tomography system," *Nuclear Instruments and Methods in Physics Research Section A: Accelerators, Spectrometers, Detectors and Associated Equipment*, vol. 873, pp. 27–35, Nov. 2017.

[11] M. Salomé et al., "A synchrotron radiation microtomography system for the analysis of trabecular bone samples," *Medical Physics*, vol. 26, no. 10, pp. 2194–2204, Oct. 1999.

[12] "NIST: X-Ray Mass Attenuation Coefficients," .

[13] "Spray Matlab Toolbox," https://www.creatis.insa-lyon.fr/~ducros/WebPage/spray.html.